Industrial Crops & Products 184 (2022) 115103

Contents lists available at ScienceDirect

Industrial Crops & Products

journal homepage: www.elsevier.com/locate/indcrop

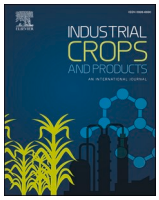

A systematic experimental study on biochar-cementitious composites: Towards carbon sequestration

Pawel Sikora [a,b,*], Paweł Woliński [c], Mehdi Chougan [d], Szymon Madraszewski [a], Wojciech Węgrzyński [e], Bartłomiej K. Papis [e], Karol Federowicz [b], Seyed Hamidreza Ghaffar [d], Dietmar Stephan [a]

[a] Department of Civil Engineering, Technische Universität Berlin, Berlin 13355, Germany
[b] Faculty of Civil and Environmental Engineering, West Pomeranian University of Technology in Szczecin, 70-311 Szczecin, Poland
[c] Faculty of Applied Sciences, Collegium Mazovia Innovative School, 08-110 Siedlce, Poland
[d] Department of Civil and Environmental Engineering, Brunel University London, Uxbridge UB8 3PH, UK
[e] Building Research Institute (ITB), 00-611 Warsaw, Poland

ARTICLE INFO

Keywords:
Cement
Biochar
Hydration
Mechanical strength
Rheology
Durability

ABSTRACT

The utilisation of biochar, the carbon negative product of pyrolysis, reduces the carbon footprint of the cementitious composites as it possesses the potential to replace the consumption of Portland cement. In a systematic investigation, biochar was used as a partial cement replacement for up to 20 wt% in both cement pastes and mortars. A comprehensive experimental framework was conducted to evaluate the impact of biochar replacement on the performance of (i) cement paste in terms of hydration kinetics, rheology, strength development, porosity, and (ii) mortars in terms of mechanical, thermal, and transport properties. In addition, the durability of developed mortars, including freezing and thawing resistance, thermal resistance, acid (corrosion) resistance, flammability, and smoke production, were examined. The results revealed that lower replacement rates of cement with biochar (up to 5 wt%) do not substantially change the performance of cementitious composites. However, incorporating biochar in higher dosages (i.e., 20 wt%) influenced the hydration process, reduced flexural and compressive strengths by 49% and 29%, respectively, and increased the water absorption coefficient by 60% compared to control specimens. The same cement mortar demonstrated the most promising freeze-thaw (i.e., 98% relative residual compressive strength), acid resistance as well as considerably lower thermal conductivity. In addition, regardless of biochar content, mortars did not exhibit flammability. Therefore, this study demonstrated that despite specific technical issues, biochar can be successfully incorporated into high dosage to cementitious composite as an alternative binder with minimum environmental impacts to improve durability and insulating performance of mortars.

1. Introduction

Concrete is the most used construction material in the world, with three tonnes per year used for every person on earth. One of the main components of concrete is Portland cement. Cement industry is responsible for approximately 8% of annual anthropogenic CO_2 emission worldwide (Andrew, 2019). One of the elements of mitigation of atmospheric CO_2 emission is the carbon sequestration strategy. It also includes incorporating carbon from atmospheric CO_2 into biomass. Biomass as an energy source is renewable and climate neutral. Many forms of biomass-to-energy conversions (e.g., pyrolysis) release no net CO_2 to the atmosphere or at least no additional CO_2 other than would have naturally taken place (Kamm, 2004).

In recent years, there has been an increase in the use of various waste materials in cementitious composites, such as industrial by-products, construction demolition waste materials, and agricultural wastes, resulting in increased physical and mechanical performance and reduced greenhouse gas emissions. Agricultural wastes are more beneficial than other waste materials in reducing waste burning in landfills, eliminating handling costs, and enhancing the material's strength while also ensuring its sustainable availability (van der Lugt et al., 2006). The natural inclusion of biomass, on the other hand, poses considerable

* Corresponding author at: Department of Civil Engineering, Technische Universität Berlin, Berlin 13355, Germany.
E-mail address: pawel.sikora@zut.edu.pl (P. Sikora).

https://doi.org/10.1016/j.indcrop.2022.115103
Received 14 March 2022; Received in revised form 8 May 2022; Accepted 15 May 2022
Available online 26 May 2022

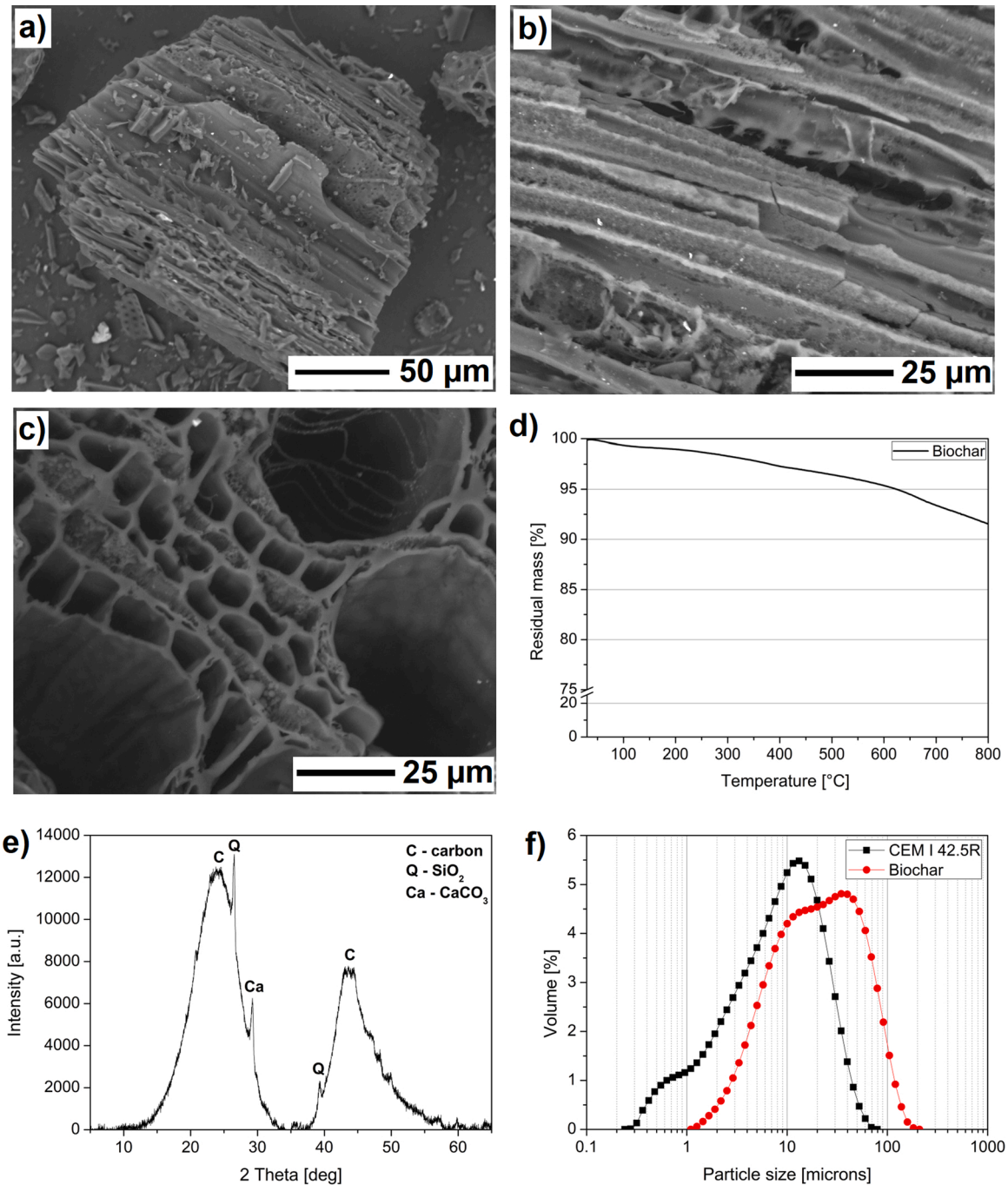

Fig. 1. Characteristics of biochar: (a-b) SEM micrographs of the outer surface, (c) cross-sectional view, (d) TG-curve, (e) XRD pattern and, (f) particle size distribution in comparison to cement.

concerns of long-term durability (Kriker et al., 2008). Plants used as biomass sources are mainly wooden crops like switchgrass, miscanthus, willow shrubs, hybrid poplar or eucalyptus (Clifton-brown et al., 2004; Gaunt and Lehmann, 2008; Kamm, 2004; Roberts et al., 2010; Volk et al., 2004). Biochar is the carbonaceous product obtained by the heat treatment of biomass under limited or no oxygen, called pyrolysis process, which is the most widely used method for producing biochar. There are two categories of pyrolysis, 1) slow and 2) fast, based on the heating rate and residence time (Murugan and Gu, 2015). Slow pyrolysis, also known as traditional carbonisation, generates biochar by heating biomass for a long residence time at a low temperature of around 400 °C in the absence of oxygen. Slow pyrolysis produces 35% of biochar from biomass, 25% of tar, 25% of non-condensable gases, and 15% of losses. This method is an uncomplicated, reliable, and low-cost method for producing biochar on a small scale (Song and Guo, 2012; Tomczyk et al., 2020). However, in the fast pyrolysis method, biochar is produced at a relatively high heating temperature of 500–1000 °C in a short residence time. This pyrolysis method provides only 12% of biochar from biomass (Bridgwater, 2012).

According to the zero-waste policy, biochar as a carbon-rich yield from pyrolysis has to be reused and neutralised in the environment. One of the most important applications is a soil amendment. It can improve soil health and structure, increasing fertility and agricultural productivity (Lehmann et al., 2006). It can also be used as an adsorbent in wastewater treatment (Shen et al., 2018; Yang et al., 2019).

Biochar addition as a cement replacement can reduce the carbon

footprint of cementitious materials (Restuccia et al., 2020). Biochar is also able to capture carbon in a stable form in buildings and at the same time, it can increase the recycling rate of the construction sector (Liu et al., 2020; Sirico et al., 2020). It has been reported that the carbon capture and storage of biochar inclusion as a feedstock accounts for 62%– 66% of the total reduction in emissions of greenhouse gas (Roberts et al., 2010). Another advantage of biochar influencing CO_2 emission is its low thermal conductivity. The pores in biochar break thermal bridging within the concrete and, therefore, ensure improved insulation of buildings. This is important for reducing energy consumption in heating or cooling buildings (Gupta et al., 2017).

The influence of biochar addition on concrete and mortar properties was the subject of many studies. A low amount (0.5–2.5 wt%) of biochar added to cement can improve its mechanical properties – compressive strength and flexural strength (Ahmad et al., 2015; Restuccia and Ferro, 2016; Suarez-Riera et al., 2020; Wang et al., 2020). In addition, it can also reduce water penetration (Gupta et al., 2018). There is limited information in the literature about durability properties (i.e., frost resistance, acid resistance etc.) of cementitious materials with biochar addition. Furthermore, it is crucial to evaluate the influence of higher amounts (5 – 15 wt%) of added biochar on cement-based material properties. Few publications (Asadi Zeidabadi et al., 2018; Gupta et al., 2018; Sirico et al., 2020; Wang et al., 2020) show that the increase of biochar decreases the compressive strength. Nevertheless, biochar can be used for other purposes. Biochar has low thermal conductivity (Gupta et al., 2017), so its addition to cementitious composites can help to fulfil new wall insulation requirements.

To the best of the author's knowledge, no study has been conducted on including relatively high quantities of biochar (i.e., up to 20% by weight) as a replacement for Portland cement. There is a lack of available data related to the durability characteristics (acid resistance, freezing and thawing, thermal resistance), thermal conductivity, transport properties (water absorption and open porosity) as well as the flammability of the material. Therefore, a series of experiments on biochar-engineered cementitious composites (both paste and mortar) for various replacement ratios of Portland cement are carried out in this study. The research is subdivided into two parts: microscale evaluation, which characterises the physical and chemical characteristics of biochar particles, as well as mesoscale examination, which evaluates the impact of biochar in cementitious composites in terms of fresh, hardened and physical properties with a focus on durability characteristics.

2. Materials and mixture composition

2.1. Materials

Ordinary Portland Cement (OPC) CEM I 42.5 R, produced by Heidelberg Cement, Germany, was used to produce cement pastes and cement mortars. Tap water conforming to EN 1008 and quartz sand (< 2 mm) conforming EN 196–1 were used along with wood chip biochar from the Polish company Fluid S.A. (Sędziszów, Poland). The biochar was ground in a planetary mill for 30 s before use. Bulk density and compacted bulk density of biochar were determined to be 0.30 g/cm^3 and 0.38 g/cm^3, respectively.

Fig. 1 presents the morphology of the outer and inner sections of biochar particles. Biochar possesses an extremely complex network of pores and channels, together with a fibrous surface. Honeycomb-like pore structures can be distinguished due to the release of volatiles from the feedstock (Fig. 1c). SEM micrograph shows that macro-pores range between 2 and 30 μm with thin walls ranging from 1 to 2 μm in thickness. Past studies reported that micro-pores and macro-pores in biochar are active in water absorption and retention and thus beneficial for retaining and storing moisture (Shafie et al., 2012).

The thermogravimetric analysis (TGA) performed with TG 209 Tarsus F3 (Netzsch) instrument showed that biochar was thermally stable in a nitrogen atmosphere with a residual mass of 92% (Fig. 1d).

Table 1
Cement paste (B series) and mortars (BM series) mixture composition ratios.

Mix	CEM I 42.5 R	Biochar	Water	Quartz sand
B0	1.00	0.00	0.5	–
B2	0.98	0.02	0.5	–
B5	0.95	0.05	0.5	–
B10	0.90	0.10	0.5	–
B20	0.80	0.20	0.5	–
BM0	1.00	0.00	0.5	3
BM2	0.98	0.02	0.5	3
BM5	0.95	0.05	0.5	3
BM10	0.90	0.10	0.5	3
BM20[a]	0.80	0.20	0.5	3

[a] BM20 mixture contains 1.4% of superplasticizer (by binder weight)

XRD was used to study the degree of carbon ordering and crystallinity of biochar samples (Fig. 1e). The broad peak at 23.5° is due to the crystal plane index C(002), which, in turn, is related to the parallel and azimuthal orientation of the aromatic and carbonised structure. The sharp peak indicates a high degree of orientation. Moreover, the high symmetry of the C(002) peak indicates the absence of γ-bands linked to amorphous and aliphatic structures (Lu, 2002). Another broad peak is observed at 43.5°, assigned to C(100) diffractions of graphitic and hexagonal carbons, which reflects the size of the aromatic lamina (Mansuri et al., 2018). The sharp C(100) peak indicates a high degree of aromatic ring condensation. The results showed reflections on the XRD spectrum at the 2θ angle of about 26, 29, 39 and 57 degrees. Small peaks at 26 °, 39° and 57° are due to quartz (SiO_2) (Bashir et al., 2018; Mohan et al., 2018). A characteristic peak at 29° attributed to the $CaCO_3$ crystal plane (Cao et al., 2020; Mohan et al., 2018). Particle size distribution performed with laser diffraction analyser (Malvern Mastersizer 2000, UK) showed that biochar was slightly coarser than cement particles with D50 and D90 equal to 22 μm and 74 μm, respectively (Fig. 1f).

2.2. Mixture composition

In the first stage, cement pastes with a fixed water-binder (w/b) ratio of 0.5 were produced. Cement was replaced with biochar at 2%, 5%, 10%, 15% and 20% by weight and specimens were designated as B2, B5, B10, B15 and B20, respectively. Moreover, control cement paste designated as B0 was produced. In the second stage, quartz aggregate was introduced to the cement paste to produce cement mortars with binder-water-aggregate ratio equal to 1:0.5:3. Cement mortars containing 2%, 5%, 10% and 20% by weight of cement with biochar replacement were produced. Cement mortars were designated as BM2, BM5, BM10 and BM20, while the control specimen was designated as BM0. To ensure appropriate workability of BM20 mortar, a BASF MasterRheobuild 1021 plasticiser was used. Mixture compositions of cement pastes and mortars are presented in Table 1.

2.3. Mixing process

A standard mixer complying with EN 196–1 was used to prepare the cement pastes. For the control mix, cement and water were mixed using the following procedure: (1) slow mixing – 30 s, (2) fast mixing – 1 min, (3) pause – 1 min, (4) fast mixing – 1 min. For other mixes, cement and biochar were dry mixed for 30 s to ensure a homogeneous distribution of fine particles was achieved. After that, the same procedure as the control mix was conducted to produce the pastes. After mixing, the 20 × 20 × 20 mm^3 cubes were cast. Cement mortars were produced with a standardised mixing procedure according to EN 196–1, and 40 × 40 × 40 mm^3 and 40 × 40 × 160 mm^3 specimens were cast. After 24 h, specimens were demolded and stored in a climate chamber with a relative humidity of 95% at room temperature (20 ± 1 °C) until the day of testing.

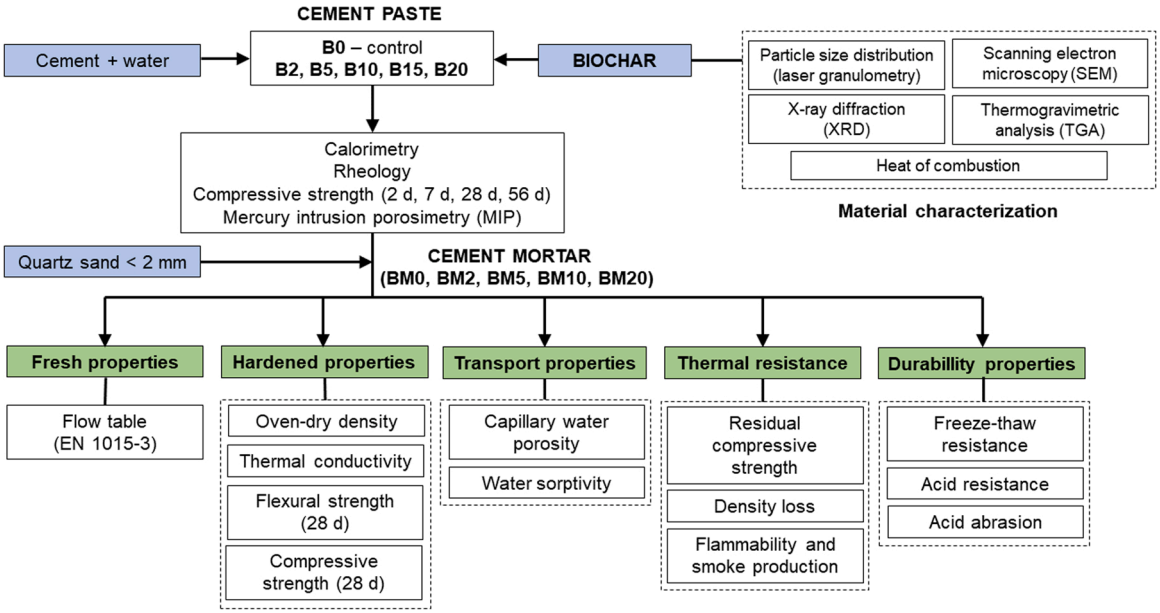

Fig. 2. Experimental framework with all the tests performed on specimens.

3. Experimental plan and methodology

The experimental protocol is depicted in Fig. 2 with all the details and steps to investigate the aims and objectives of this study.

3.1. Calorimetry

The calorimetry measurement was performed using an isothermal heat flow calorimeter (MC-CAL/100 P, C3 Prozess- und Analysetechnik). For evaluating the hydration kinetics with calorimetry, 5 g of water was mixed with 10 g of binder (cement and biochar) and the hydration heat of the samples was measured for 6 days. The heat flow and cumulative heat were determined.

3.2. Rheological measurements

The rotational rheometer Rheotest RN4 with concentric cylinder geometry was used to determine the rheological parameters of cement pastes. The following procedure was applied: (i) pre-shearing for 30 s at a constant shear-rate of 100 s^{-1}, (ii) determination of shear-stress as a function of shear-rate, from 100 s^{-1} to 0.1 s^{-1}, with 20 points distributed evenly along a logarithmic scale, for a total of 300 s. The rheology test was performed according to the methodology of Haist et al., (2020), with certain modifications. Among several fitting models, including the Modified-Bingham (MBM) and Herschel-Bulkley (HB) models, which have been reported for the rheological assessment of cementitious composites, the Modified-Bingham model was employed to extract the plastic viscosity (η_p) and yield shear stress (τ_0) of each mixture (Eq. 1). This method was chosen to improve the fitting precision, and the non-Newtonian and pseudoplastic character of the cementitious composites.

$$\tau = \tau_0 + \gamma \times \eta_p + c\gamma^2 \quad (1)$$

3.3. Consistency

The consistency of fresh cement mortars was determined with the flow table method conforming to EN 1015–3.

3.4. Oven-dry density and thermal conductivity

Oven-dry density and thermal conductivity of cement mortars were measured after 28 days of curing. For this purpose, three 40 × 40 × 160 mm^3 prisms of each type of mortar were oven-dried at 105 °C at least for 24 h (until reaching a constant mass). Afterwards, three mass measurements were performed, with the mean value being selected as the dry density. The thermal conductivity of cement mortars was determined with the transient plane source method (TPS) conforming to ISO 22007–2 using a Hot Disk TPS 2200 device (Hot Disk AB, Sweden). Thermal conductivity was measured using a Kapton-insulated sensor placed between two dried identical prismatic mortar specimens. Each mix design was tested on three groups of specimens, with the mean value considered in each case.

3.5. Mercury intrusion porosimetry (MIP)

MIP was utilised to determine the pore size distribution of cement pastes after 28 d of curing. Before measurement, small-cored samples drilled out from the middle of the specimens were immersed in isopropanol to stop hydration. Afterwards, specimens were subsequently freeze-dried before testing. The measurement was performed using a Pascal 140 and 240 series (Thermo Scientific) mercury intrusion porosimeter. The mercury density was 13.5450 g/mL, the surface tension was taken as 0.48 N/m, and the selected contact angle was 140°.

3.6. Mechanical properties

The flexural and compressive strengths of cement-based composites were determined with a digital crushing machine (Toni Technik Baustoffprüfsysteme GmbH, Berlin, Germany), conforming to EN 196–1. Six cubes in size of 20 × 20 × 20 mm^3 of each type of cement paste were tested after 2, 7, 28 and 56 days, with the mean value taken into consideration. Similarly, after 28 d of curing, six 40 × 40 × 160 mm^3 mortar prisms were used to determine the flexural strength, while afterwards, obtained halves were used to determine the compressive strength.

3.7. Transport properties

The capillary water porosity of 40 × 40 × 160 mm^3 mortar prisms

was determined using the water displacement method, based on the Archimedes principle. The water absorption coefficient of the mortars was determined from the results of the water sorptivity test, based on the partial immersion method conforming to EN ISO 15148. Before the measurement, the sides of three 40 × 40 × 160 mm^3 prisms of each type of mortar were sealed with hot paraffin wax. During measurement, the water level was kept constant at about 5 mm above the highest point of the bottom side of the prism. A detailed description of tests can be found in (Abd Elrahman et al., 2019).

3.8. Freeze and thaw resistance

Freeze and thaw resistance was determined according to the Polish Standard PN-85-B-04500. After 28 d of curing, cubic specimens (40 ×40 ×40 mm^3) were oven-dried at 105 °C for at least 24 h (until constant mass) and weighed. Afterwards, specimens were saturated in water for 7 days, after which they were exposed to 25 freeze-thaw cycles, each lasting 8 h, during which the samples were frozen for 4 h in air at − 20 °C and then thawed for another 4 h in water at 20 °C. The reference samples remained in water, at a temperature of 20 °C, without exposure to freezing and thawing. Specimens were dried, and their mass loss and compressive strength loss were determined. The freezing and thawing cycle is depicted in Fig. S1 (Supplementary Materials).

3.9. Thermal resistance

The heating of the mortar cubic specimens (40 ×40 ×40 mm^3) was performed using a medium-temperature furnace after 28 d of curing. Specimens were exposed to a temperature of 300 °C, 450 °C, 600 °C and 800 °C. Before the measurement, specimens were dried for 16 h at a temperature of 65 °C, to remove the excessive moisture of specimens. In the first stage, a constant heating rate of 4 °C/min was maintained in the furnace. After reaching the desired temperature, the samples were left in the furnace for 2 h to stabilise the temperature over their entire cross-section. Subsequently, specimens were taken out from the furnace and left to cool in ambient laboratory conditions for approximately 6 h and transferred to a sealed container. Compressive strength was tested 24 h after removing specimens from the furnace. Relative residual compressive strength (RRCS) was calculated following Eq. 2.

$$RRCS\ [\%] = \frac{F_{c,t}}{F_{c,28}} \times 100 \quad (2)$$

Where $F_{c,t}$ is the compressive strength of specimen at selected heating temperature and $F_{c,28}$ is the compressive strength of specimen non-heated specimen at 28 days.

A similar testing procedure was applied to evaluate the specimens' mass loss. However, all specimens were dried until constant mass and weighed before the heating. Six cubes of each mortar type were subjected to elevated temperatures and mean values were taken as a representative.

3.10. Flammability and smoke production

The flammability of cementitious mortars was assessed following ISO 1716 and ISO 5660–1 to determine the gross heat of combustion and the dynamic production rate of smoke and heat when exposed to heat, respectively. Combining these tests makes it possible to establish whether the material can be ignited and generate smoke and other products when exposed to fire. The results of the tests could also be used to estimate the euro class for the building material's fire resistance. To use the product in fire-rated barriers and separations, the maximum response to fire class (A1, A2) may be required.

3.10.1. ISO 1716 Determination of the gross heat of combustion

In this test, a given mass specimen was combusted in an oxygen environment under constant volume and standard conditions. The calorific value (i.e., gross heat of combustion) was calculated based on the rise in water temperature in the calorimetric vessel used to cool the sample. Heat losses and the latent heat of vaporisation of water were used to calculate the amount of heat.

For each mixture composition, this test was repeated three times. Each time, a 0.5 g sample was powdered and mixed with an equal amount of a combustion aid (benzoic acid) before being placed in the bomb, filled with oxygen and compressed. A firing wire in contact with the powder initiates the combustion process. In this case, the biochar cement mortar can be considered as a homogeneous material for which the criteria are PCS ≤ 2 MJ/kg or PCS ≤ 3 MJ/kg for classes A1 and A2, respectively. This test was performed three times for each mixture composition.

3.10.2. ISO 5660–1 Cone calorimeter

The cone calorimeter test was used to assess the cementitious mortar's fire and smoke behaviour based on a relatively small-sized material sample (sample size of 0.01 m^2). This test determines materials' ignitability, combustibility, smoke production, and toxic gas production. Although test methods requiring large samples (i.e., Single Burning Item, the sample size of 2.25 m^2) are needed to confirm material properties in a product certification process, the cone calorimeter results have been found to correlate well. This method can estimate the performance of materials not exhibiting lateral flame spread in the SBI test.

Samples were placed on a load cell holder and heated by a conical-shaped heat source with a constant heat flux of 50 kW/m^2. When volatile gasses were emitted from the sample, an electrical spark ignited them. The combustion gasses were collected with an exhaust hood where the temperature, pressure, opacity, O_2, CO, CO_2 and H_2O measurements were taken. By determining the O_2 concentration in the combustion products, it is possible to determine the heat release rate per unit of area of the sample. The total heat release (THR) fire growth rate (FIGRA) are used to correlate the results of the cone calorimeter with SBI results.

3.11. Acid resistance tests

To determine the acid resistance of mortars, two types of tests were conducted. The first test was performed according to the modified version of the DIN 19573 acid resistance test. The second was the LPI acid abrasion test, proposed by Petersen and Lohaus (Petersen and Lohaus, 2006). Both tests were performed on samples after 56 days of curing.

3.11.1. Modified DIN 19573 test

The resistance of mortar to acid attack in the DIN acid resistance test was studied by complete immersion of specimens in 4 L sulfuric acid solution (pH 3) for 4 weeks. For every mixture composition, 5 samples (40 ×40 ×80 mm^3) were used. Samples of all mixtures were stored in separate tanks. To maintain the pH value as close to 3 as possible, 3 wt% sulfuric acid was automatically added to the solution when its pH value elevated > 3.1. The volume of acid added was recorded continuously. The pH value was measured every 5 min. To avoid Ca^{2+} ions saturation, the solution was renewed every 2 days for the first 2 weeks, then every 3 days for the last 2 weeks. Specimens were taken out of the solution after 28 days of acid exposure, wiped gently and weighted. The acid resistance was assessed by measuring the weight loss of specimens after acid exposure.

3.11.2. LPI test – acid abrasion test

To simulate close to real-life situations of acid attack including an abrasion wetting and drying cycles of corrosion, the LPI acid abrasion test was carried out for 4 weeks. Samples (40 ×40 ×160 mm^3) rotate while immersed in 12 L acid solution (pH 3) with a rotational speed of 0.4 rpm. One side of the samples is exposed to brushing, which occurs at

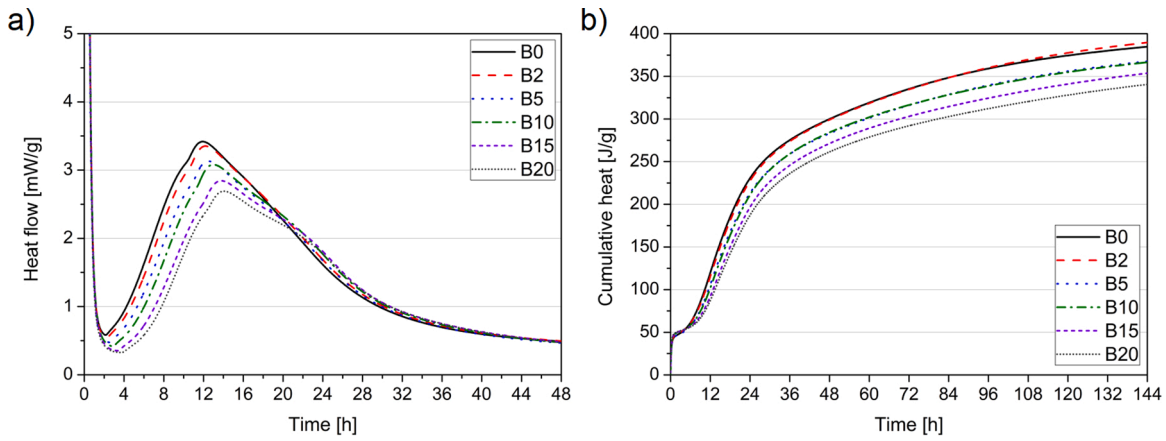

Fig. 3. Heat flow up to 48 h (a) and cumulative heat up to 144 h (b) per gram of solid (binder).

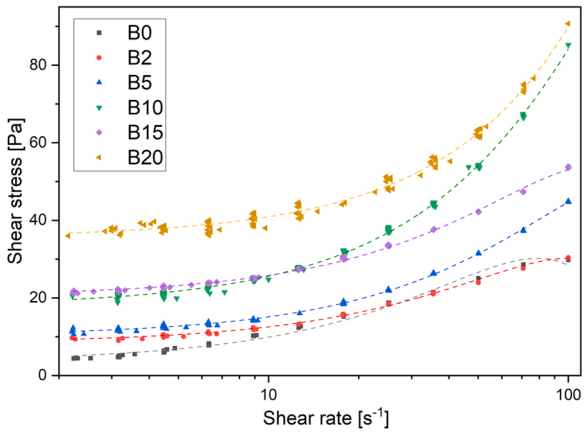

Fig. 4. Shear stress versus shear-rate.

every rotation. Acid titration, pH maintaining and renewing procedure was kept constant as in the DIN acid resistance test. Once a week, specimens were taken out of the solution, wiped gently and weighted. After 28 days, the samples were removed from the acid solution dried in room conditions. The acid resistance was assessed by the differences in the weight of specimens before and after the acid attack.

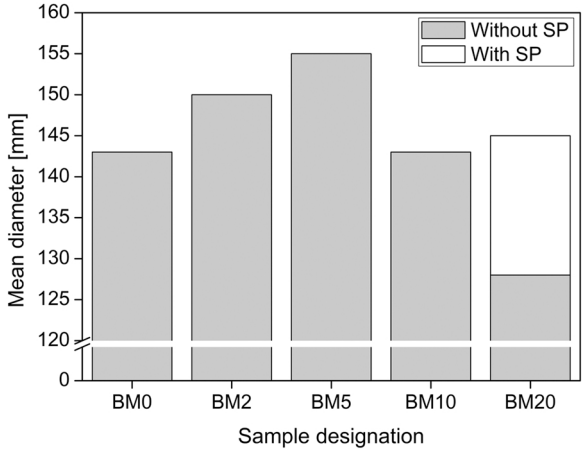

Fig. 5. Consistency of fresh mortars measured with flow table test. Note: Mean diameter of BM20 specimen was tested for same mortars with and without superplasticiser.

4. Results and discussion

4.1. Calorimetry

The results of the calorimetric study are presented in Fig. 3. A noticeable difference in the hydration kinetics of specimens containing biochar can be observed. The increment of cement replacement with biochar delays the exothermic peak appearance (Fig. 3a). The occurrence of the exothermic peak was delayed respectively by 15, 33, 61, 111 and 127 min for specimens B2, B5, B10, B15 and B20 compared to B0. Similarly, the peak value was almost linearly decreased by 2.0, 8.4%, 9.9%, 16.8% and 21.3% for specimens B2, B5, B10, B15 and B20, respectively, compared to B0. The replacement of cement with biochar also resulted in a decrement in the cumulative heat of the binder (Fig. 3b). The total cumulative heat values after 144 h of B5, B10, B15 and B20 were 4.5%, 4.8%, 8.1% and 11.5% lower, respectively, compared to B0. On the contrary, specimen B2 exhibited a comparable value of total cumulative heat than B0, only 1.3% higher.

The effect of biochar on hydration kinetics depends on a few factors, including its chemical composition, pyrolysis process conditions and its fineneses (Tan et al., 2021b). Generally, low dosages of fine biochar particles (finer than cement) have either a substantial effect on the acceleration of the cement hydration process by promoting the nucleation and growth of hydration products or a negligible effect on hydration kinetics (Gupta and Kua, 2019). Similarly, in the present study, low biochar dosage (B2) exhibited a marginal effect on the cement hydration process, which can be attributed to the relatively coarser size of biochar when compared to cement particles (Fig. 1f); thus, the potential nucleating effect was limited. Higher replacement rates of cement with biochar resulted in the delayed occurrence of silicate peak (Fig. 3a) and decreased cumulative heat released after 144 h (Fig. 3b) due to lower available cement content in the mixture.

4.2. Rheology of cement paste

Although cementitious composites' inadequate workability leads to poor mechanical strength and durability, the rheological behaviour of these composites as an accurate workability scale has been rarely considered (Berra et al., 2012; Chougan et al., 2019; Wang et al., 2017). The flow curves for various mixes are presented in Fig. 4, which confirms the substantial influence of the biochar replacement dosage on the rheology of fresh pastes. Modified-Bingham fitting model was applied to the data obtained from the rheometer to extract the rheological parameters. Rheological characteristic, i.e., yield shear stress (τ_0), was used to define the flow behaviour of each mixture. According to several research studies, plastic viscosity is linked to the material's cohesiveness and pumpability, whereas workability is related to yield stress (Maharaj

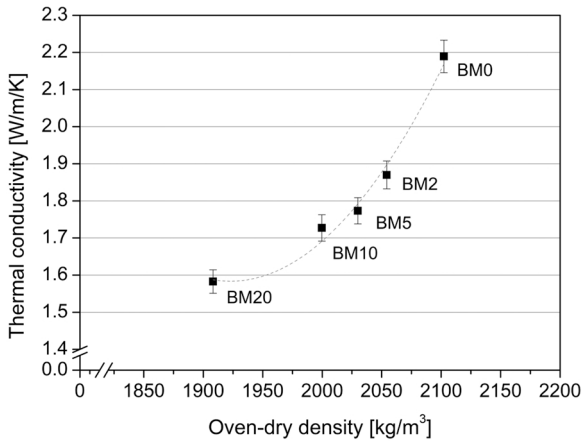

Fig. 6. Thermal conductivity of mortars tested through Transient Plane Source (TPS) method as a function of oven-dry density.

et al., 2015). As a result, in this study, the yield shear stress was evaluated based on the conventional application of these materials.

The results confirm that increasing the biochar replacement ratio induces a progressive increase in τ_0 from 8.4 Pa for B2 to 10.3 Pa, 17.9 Pa, 20.48 Pa, and 35.6 Pa for B5, B10, B15, and B20, respectively. All of which are higher than the τ_0 value registered for the control sample (i.e., 3.6 Pa). This might be attributed to the irregular geometry of biochar particles preventing lubrication or ball bearing effect, and high carbon content in biochar raises water retention capacities, which reduce workability. Moreover, biochar particles' large surface area and porous structure lead to a high-water absorption rate that can absorb a significant proportion of the mixing water required for workability (Choi et al., 2012; Danish et al., 2021; Igalavithana et al., 2017; Ofori-Boadu et al., 2017).

4.3. Fresh properties assessment of cement mortar through flow table test

The workability of fresh mortars has been depicted in Fig. 5. Up to 10 wt% of biochar replacement, no marginal differences in the consistency of the mortar was reported, which is in line with rheology test results (Fig. 4). Specimens BM2 and BM5 exhibited minimally higher spread flow, while BM10 exhibited comparable flow to BM0. On the contrary, BM20 significantly lost workability when superplasticiser was not added to the mixture. After including superplasticiser for BM20, similar consistency to BM0 was reached. Due to the highly porous structure of biochar and its hydrophilic nature, there is a higher water demand. Therefore, with the increasing biochar replacement rate, the inclusion of plasticising agents is unavoidable (Tan et al., 2021b).

4.4. Density and thermal conductivity

The replacement of cement with biochar led to a significant decrement in the thermal conductivity of mortars (Fig. 6). The density of the cementitious composites has a significant effect on the thermal conductivity of the material (Asadi et al., 2018; Strzałkowski et al., 2021). Therefore, the replacement of cement with substantially lighter and highly porous biochar resulted in a noticeable decrement of oven-dry density and, therefore, thermal conductivity. A gradual density loss as a result of biochar dosage increase was reported by Cuthbertson et al., (2019). Despite the clear trend between thermal conductivity and density of cement mortars, a substantial decrease of thermal conductivity were observed even for mortars with a low dosage of biochar (BM2). As reported by Akinyemi and Adesina, (2020) this phenomenon could be attributed to the highly porous structure of biochar, which can disrupt the thermal bridges and serve as a barrier for phonon transport within the cement matrix. Therefore, the BM2 specimen exhibited almost 15% lower thermal conductivity than the BM0 specimen. Incorporation of 20 wt% biochar (BM20) resulted in the reduction of thermal conductivity by 28% from 2.19 W/m/K (BM0) up to 1.58 W/m/K.

Table 2
Basic parameters of pore structure measured by MIP.

Sample designation	B0	B2	B5	B10	B15	B20
Porosity by Hg intrusion [vol.-%]	24	25	26	27	30	29
Average pore diameter [nm]	36	42	44	49	40	41
Median pore diameter [nm]	62	77	81	162	77	85

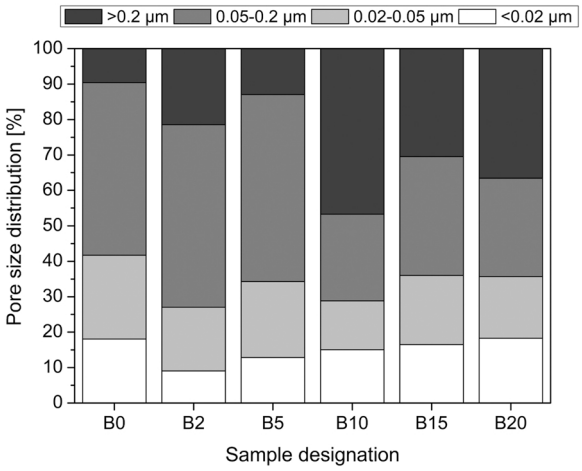

Fig. 7. Pore size distribution of cement pastes measured by MIP.

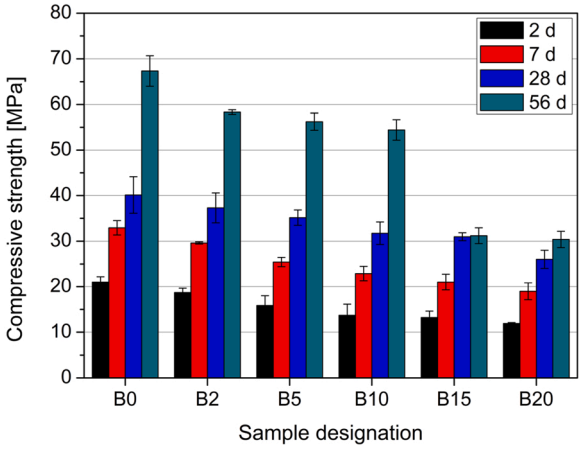

Fig. 8. Compressive strength after 2, 7, 28 and 56 d of hydration of cement pastes.

4.5. Mercury intrusion porosimetry (MIP)

Table 2 presents the basic porosity characteristics of cement pastes obtained from MIP measurement. An increment in biochar replacement rate resulted in a gradual increment in paste porosity and higher biochar contribution. Specimen B15 exhibited a porosity of 30 vol% followed by B20 with porosity of 29 vol% compared to 24 vol% reported for control cement paste (B0). These results are in line with an increase in the average and median pore diametre of specimens containing biochar compared to the control sample. Pore size distribution analysis (Fig. 7) shows that up to 5 wt% cement replacement with biochar, no substantial alteration in the pore size distribution can be reported, however with higher replacement dosage, coarser pores are found in the specimen.

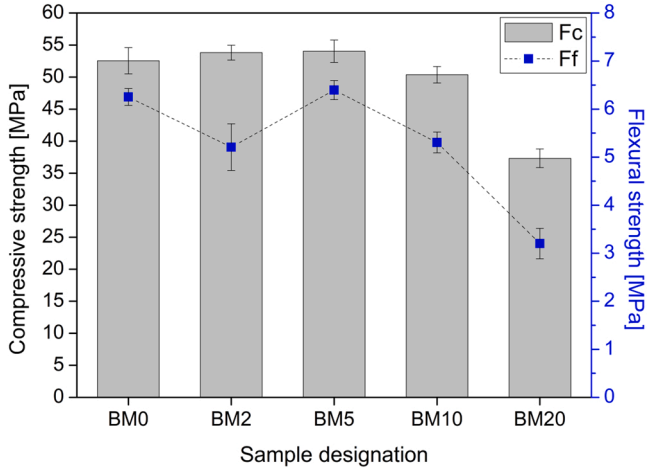

Fig. 9. Flexural strength (F_f) and compressive strength (F_c) of cement mortars after 28 days of curing.

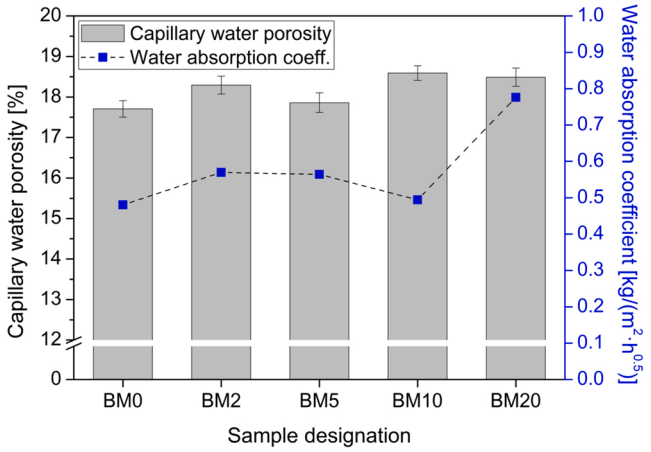

Fig. 10. Capillary water porosity and water absorption coefficient of mortars.

A recent study conducted by Praneeth et al. (2021), has used X-ray micro-computed tomography to evaluate the microstructural features of cement mortars containing up to 40 wt% replacement of sand, showed nearly a five-fold increase in the porosity of the samples, from 2.5 vol% (control) to 12 vol% for samples which had 40 wt% of biochar. On the contrary, marginal increment of porosity was reported when sand was replaced with 20 wt% of biochar.

4.6. Mechanical performance of cement pastes and mortars

The strength development of cement pastes containing various dosages of biochar is presented in Fig. 8. It can be clearly noticed that from the early days of hydration (2 d and 7 d), specimens containing biochar exhibit gradual strength decrement along with increasing content of biochar. After 28 d of curing, B2, B5, B10, B15, B20 exhibited 7%, 12%, 21%, 23% and 35% lower compressive strength than the control, B0 specimen. After 56 d, the discrepancy between compressive strength values of pristine and biochar-modified specimens was significantly increased, especially with high dosages of cement replacement with biochar (from 15 to 20 wt%). Specimens B2, B5, B10, B15, B20 exhibited 13%, 16%, 19%, 54% and 55% lower compressive strength values than B0 specimens. Compressive strength results confirm that the presence of biochar generates a more porous cementitious matrix attributed to its coarser particle size distribution and high porosity, resulting in a weaker cement paste microstructure and lower mechanical performance.

Compressive strength evaluations performed on cement mortars (Fig. 9) showed that up to 10 wt% of biochar replacement led to no substantial changes in the compressive strength. BM2 and BM5 specimens exhibited minimally higher compressive strength (2% and 3%, respectively), while BM10 exhibited 4% lower compressive strength than the control sample, BM0. Exceeding the biochar dosage up to 20 wt % (BM20) resulted in the reduction of compressive strength by 29%. The mechanical performance of cement mortars reported after 28 d of curing differs from the results reported for cement pastes (Fig. 8). Despite chemical interactions with cement, lower dosages of fine biochar (finer than cement) might exhibit a filling effect resulting in compaction (densification) of cement matrix and, hence, strength improvement (Dixit et al., 2019; Park et al., 2021; Praneeth et al., 2021). In this study, the beneficial effect of biochar on the mechanical performance of cement pastes was limited, as biochar used was coarser than cement particles (Fig. 1f); therefore, a more porous matrix was produced (Table 2). On the contrary, due to the inclusion of sand into cement mortar, the microstructure of cement mortar was more heterogeneous; thus, finer particles of biochar could sufficiently fill in the voids in the cement matrix. Therefore, the mechanical performance of mortars with a low biochar dosage remained comparable to that of BM0 (control) specimen. However, when a higher replacement rate of cement with biochar was introduced to the mixture, substantial strength reductions were observed, which might be due to high porosity and water absorption of mortars with higher dosages of biochar, leading to the production of the porous microstructure of cementitious composite.

Similiarly, replacement of cement with biochar resulted in noticeable alteration in the flexural strength of mortars. The incorporation of up to 5 wt% of biochar exhibited a slightly lower or comparable flexural strength than the control sample. Incorporation of 10 wt% (BM10) and 20 wt% (BM20) resulted in substantial flexural strength loss of 16% and 49%, compared to BM0. Due to the inhomogeneity of biochar, in comparison to the cementitious matrix, when high quantities are introduced to the mix, a weak interface between biochar and the cementitious matrix is produced, leading to agglomeration of material and formation of a weaker interfacial zone. Worth noting that, due to the low strength of biochar itself (Dixit et al., 2021) and increased porosity of cement matrix due to the presence of high volumes of biochar, the cementitious composite is more susceptible to cracking under loading (Dixit et al., 2019).

4.7. Transport properties

Fig. 10 presents the capillary water porosity and water absorption coefficient calculated from the sorptivity measurements. In general, all specimens containing biochar exhibited higher values of capillary water porosity than the control mix (BM0), with the lowest value reported for BM5. The highest increment of capillary water porosity by 4.4% and 5.0% was reported for specimens BM20 and BM10, respectively. An increase in water absorption coefficient was found for BM2 and BM5. Surprisingly, specimen BM10 exhibited a slightly lower coefficient value than BM0. A significant rise by 60% in the water absorption coefficient of the BM20 specimen was found compared to BM0.

The observed trend in increased transport properties of cement mortars could be attributed to the highly porous surface of biochar. Biochar has an irregular pore structure and consists of various pore sizes, ranging from 2 to 30 μm (according to SEM study, Fig. 1), which is most beneficial in retaining and storing moisture. When a low dosage of biochar is included (usually ≤2 wt%), such phenomena can be beneficial for the internal curing effect. On the contrary, high dosages of biochar act as a hygroscopic filler, leading to improved water absorption and retention capability. According to Park et al. (2021) biochar's high porosity and large surface area enhance hygrothermal performance temperature. Consequently, the material's porous structure could absorb and release water vapour in response to changes in relative

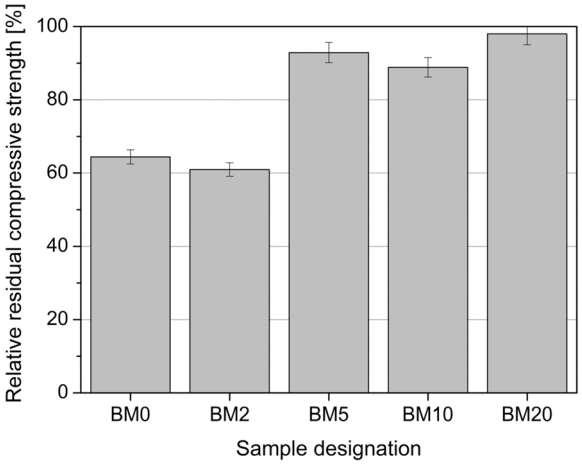

Fig. 11. Relative residual compressive strength of mortars after 25 freeze-thaw cycles.

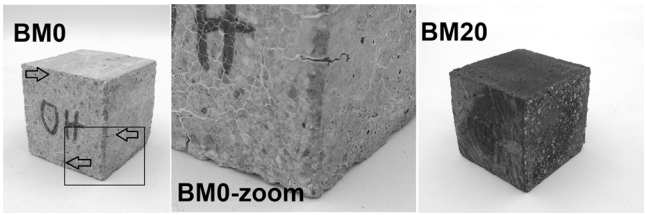

Fig. 12. Visual inspection of BM0 and BM20 mortar specimens (40×40×40 mm^3) after 25 freeze-thaw cycles.

humidity in the living environment. Tan et al. (2021a) reported that macro-pores in biochar particles could retain free water; thus, permeable concrete containing 5 wt% of biochar exhibited higher capillary suction and water storage. Furthermore, as reported by Gupta and Kua (2018) the release of absorbed water back into the medium from the biochar pores can also promote cement hydration.

4.8. Freezing and thawing resistance

Fig. 11 depicts the results of the relative residual compressive strength (RRCS) of samples with and without biochar following 25 freeze-thaw cycles. The RRCS value was decreased from 65% for the control sample to 61% for BM2. The slight reduction in freeze-thaw resistance of the low fraction biochar replacement sample is attributed to the higher capillary water porosity and water absorption coefficient of this mixture compared to the control sample (see Section 4.7). This results in crack initiation (see Fig. 12) due to expansion of entrapped water during the freezing process (i.e., stress transfer effect), which widen and rupture the pore cavities within the composite (Wu et al., 2021). Subsequently, the inclusion of more biochar (i.e., BM5, BM10, and BM20) remarkably increased the RRCS value, reaching 93%, 89%, and 98%, respectively. This enhancement in freeze-thaw resistivity can be attributed to high volume of biochar particles which provides space for expanding water during freezing, and thus restraining the specimen from cracking. The visual inspection of BM0 and BM20 samples (see Fig. 12) also verified the ability of mortars containing biochar particles to impede the crack propagation during the freeze-thaw cycles.

4.9. Thermal resistance

Fig. 13 presents the residual compressive strength of cement mortars calculated according to Eq. 2 and the relative residual density of specimens after exposure to an elevated temperature of 300, 450, 600 and 800 °C. Concrete possess good thermal resistance up to 300 °C, with only relatively minor damage occurring. Exposure to a temperature > 300 °C can be harmful to cement-based composites, as severe decomposition of calcium hydroxide (CH) and Calcium-Silicate-Hydrate (C-S-H) gel occurs (Sikora et al., 2018). Moreover, the thermal incompatibilities between aggregate and cement paste cause an increase in matrix porosity and micro-cracking, resulting in strength losses.

At a temperature of 300 °C, differences in RRCS (Fig. 13a) were observed. The highest strength loss was obtained for specimen BM20, followed by BM0; however, the discrepancy between specimens' strength did not exceed 12%. Exposure to 450 °C resulted in similar strength loss of all specimens by 30%, except specimen BM20, which exhibited > 50% strength loss. After exposure to 600 °C, further substantial strength loss was reported showing a distinct difference between specimen's strength. Gradual decrement of strength was reported along with the increment of biochar dosage in the mixture. Specimens BM0, BM2, BM5, BM10 and BM20 possessed 48%, 45%, 45%, 36% and 28% of initial compressive strength after exposure to 600 °C. Specimens that were exposed to 800 °C lost > 80% of their initial compressive strength due to the decomposition of the main cement paste constituents (Sikora et al., 2018). Higher-strength loss of specimens containing biochar can be attributed to the ignition loss of biochar at high temperatures. As reported by Yang et al., (2021) the carbon in biochar reacts to generate CO_2 gas and escapes through pores and cracks during exposure to high temperatures and oxygen. This was also confirmed by testing the relative residual density of specimens (Fig. 13b). From 450 °C, specimens with higher biochar content exhibited higher mass loss which is attributed to the decomposition of biochar. In the case of BM2 and BM5, the differences were comparable to that of BM0 due to the relatively low contribution of biochar to the overall mass of the mortar. Incorporating biochar into the mixture resulted in changing the specimen's colour into dark grey along with biochar dosage. In contrast, after exposure to a temperature of 600 °C, all specimens exhibited the same light grey

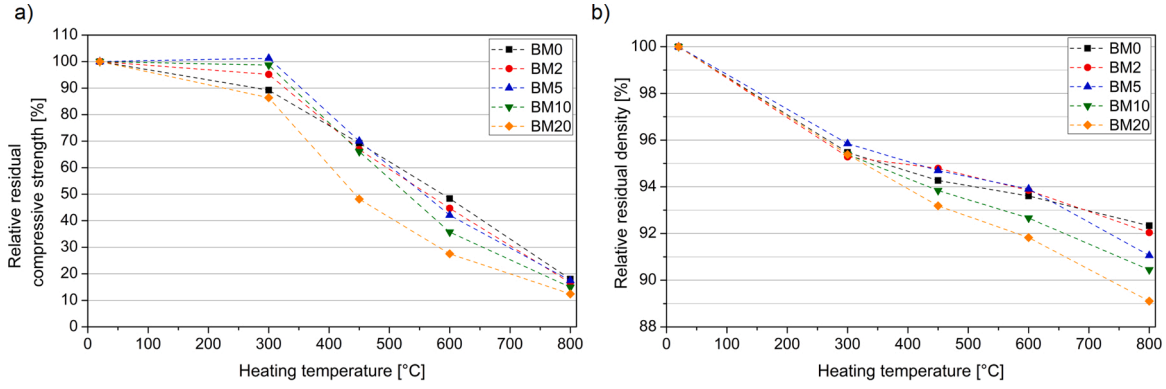

Fig. 13. Relative residual compressive strength (a) and relative residual density (b) after exposure to elevated temperatures.

Table 3
Heat of combustion (Q (PCS)) measured according to ISO 1716.

Sample designation	BM0	BM2	BM5	BM10	BM20	Biochar
$\dot{q}''(PCS)$ [MJ/kg]	-0.62	-0.59	-0.86	-0.17	0.08	18.93

colour (Fig. S2, Supplementary Materials), which confirms the loss of ignition of biochar due to oxidation of carbon. The decomposition of biochar during exposure of specimens to high-temperature results in voids in the specimen, thus weakening the skeleton of the cement matrix, which in turn reduces the compressive strength. Therefore, higher replacement rates of cement with biochar (10 wt% and 20 wt%) lead to a substantial decrement in the thermal resistance of cement mortars.

4.10. Flammability

The average results of the heat of combustion $\dot{q}''$ (PCS) determined in ISO 1716 apparatus are presented in Table 3. The heat of combustion measurement for samples BM0, BM2, BM5 and BM10 has shown negative value, which indicates that the apparatus with biochar sample has reached a lower temperature than in a calibration test without any material sample. This means that any combustion processes in the sample are insignificant compared to the sample's heat capacity. Sample B20 showed positive heat of combustion (average of 0.08 MJ/kg); however, its value was close to zero which was significantly lower than the heat of combustion of biochar sample (18.93 MJ/kg). It can be interpreted that the heat produced in the combustion of biochar component is consumed to heat the cement mortar in the mixture, resulting in net production of heat close to zero.

In the cone calorimeter test ISO 5660–1 under 50 kW/m^2 irradiance, samples with high biochar content have demonstrated some degree of flammability, i.e. they have not ignited but generated average heat flux of 1.55 kW/m^2, 4.15 kW/m^2 and 9.22 kW/m^2 for BM5, BM10, BM20, respectively. Total heat release per unit of area measured after 600 s (THR_{600}) was 1.05 MJ/m^2, 2.55 MJ/m^2, and 5.02 MJ/m^2 for BM5, BM10, BM20, respectively. Fig. 14a shows almost linear scaling of the THR with the biochar content in the mixture. For the mixtures with low biochar content, the release was below the threshold of the apparatus. Similarly, the total smoke production was scaled with the biochar content. The total production after 600 s (TSP_{600}) measured was 0.15 m^2, 0.42 m^2 and 0.65 m^2 for BM5, BM10, BM20, respectively (Fig. 14b). Both THR and TSP values can be considered very low (10 – 100 times lower) compared to combustible polymer composites (Qiu et al., 2017).

Based on the low heat of combustion, i.e., low THR and TSP values and no visible ignite, the tested mixes may fit within the A2 category of fire reaction. The average heat generation of BM20 was found to be 9.22 kW/m^2. However, it should be highlighted that this was achieved at a 50 kW/m^2 external irradiation, implying that the combustion is not self-sustaining. Though in some legislative systems, this would not qualify the material as non-combustible. Following the logic of Babrauskas, (2017) the material can be considered as not contributing to the propagation of flame, achieving the most important objective of fire safety engineering. The objective flammability of the material may also be determined with the approach of Cleary and Quintiere, (1991), through estimation of parameter b (Eq. 3).

$$b = 0.01\dot{q}'' - 1 - \frac{t_{ig}}{t_b} \tag{3}$$

where $\dot{q}''$ is heat release rate [kW/m^2], t_{ig} is the time to ignition in cone calorimeter and t_b is time of flaming. In our case the sample has not ignited. According to theory. if $b \leq 0$, then there is no significant hazard of sustained flame propagation. In the case of tested mixtures, the values of b were -0.98 to -0.91, fulfilling this requirement. Babrauskas, (2017) claimed that materials with $b < -0.4$, when exposed to 300 kW burner in ISO 9705 room/corner test, will not result in a flashover in the room. Determining if the material can contribute to flashover is also one of the goals of the SBI test, which is used in the formal assessment of the reaction to fire class. Furthermore, it was observed that only the outermost layer (approx. 10 mm in depth) of the tested specimen exhibited the combustion of the biochar component, while the rest of the sample remained intact after the test (Fig. S3, Supplementary Materials). This confirms that the contribution of the mixture to the fire may occur only in a fully developed fire, thus not being relevant for the early phases when occupant evacuation takes place.

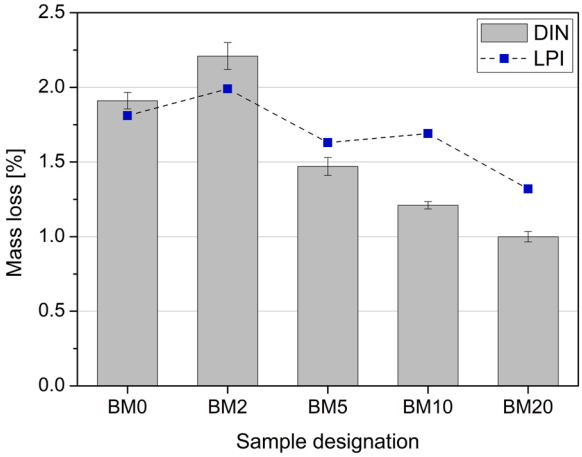

Fig. 15. Mass loss determined from two types of acid resistance tests according to modified DIN 19573 and LPI testing methods.

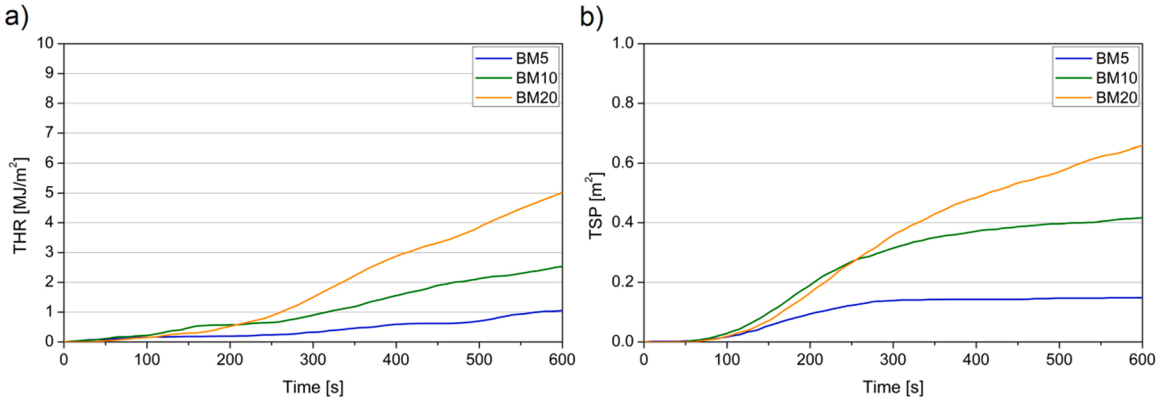

Fig. 14. Total heat release (a) and total smoke production registered for BM5, BM10, BM20.

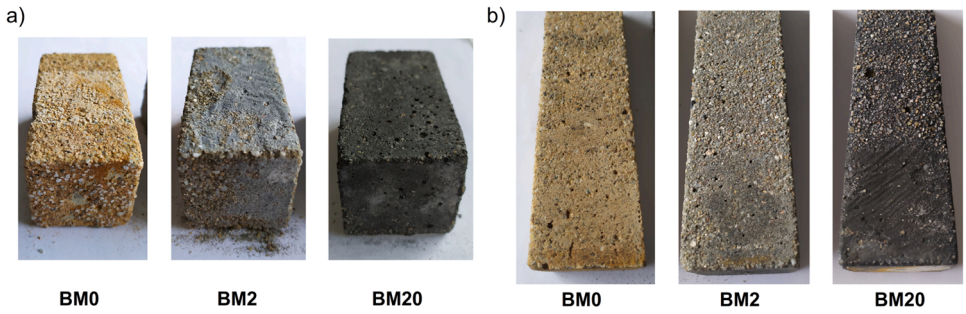

Fig. 16. Optical inspection of the selected mortar specimens (40×40×160 mm^3) after modified DIN 19573 (a) and LPI (b) acid resistance tests.

4.11. Acid durability

Fig. 15 presents the results of mass loss obtained for specimens using two acid attack methods, while Fig. 16 presents the surface of selected specimens after testing. Full images of the whole set of specimens are presented in Fig. S4 and Fig. S5 (Supplementary Materials). After 28 d of exposure to the sulphuric acid solution at pH 3 (modified DIN 19573 test), the surface of the samples exhibited brownish areas of discolouration (Fig. 16a). The lower the amount of biochar, the greater the change in samples' surface colouration. The titration data of the DIN acid resistance test show that the rate of acid consumption depends on the amount of biochar. The amount of sulfuric acid required to maintain a pH value of 3.0 was normalised to the sample surface. After 28 days DIN acid resistance test, 0.94 mmol H^+/cm^2, 0.69 mmol H^+/cm^2, 0.56 mmol H^+/cm^2, 0.55 mmol H^+/cm^2 and 0.57 mmol H^+/cm^2 of total acid were depleted by the BM0, BM2, BM5, BM 10 and BM 20 samples, respectively. After 28 days of the LPI acid abrasion test, the total amount of acid consumed by all samples was 0.95 mmol H^+/cm^2.

The mass loss result (Fig. 15) for DIN acid resistance shows that after 28 days, the highest mass loss (i.e., 2.21 wt%) was observed for BM2 samples, while the lowest mass loss of 1.00 wt% was registered for BM20 samples. It can be concluded that a decrease in mass loss is linked to biochar replacement dosage in the mortar. This phenomenon can be attributed to the reduced amount of cement in composites with biochar at the same w/b ratio.

After 28 days of the LPI acid abrasion test, the trend of mass loss was comparable to that obtained during the DIN acid resistance test. From these results, it can be gathered that 5 wt% or more of biochar replacement make mortars more susceptible to abrasion during an acid attack.

5. Conclusions

This study aimed to comprehensively characterise the impact of biochar replacement with cement in pastes and mortar specimens. There are many advantages in replacing Portland cement with alternative, more environmentally friendly sources including biochar. Our study revealed that replacing cement with biochar results in a decrement in the heat of hydration of binder. Only in the case of a low replacement level (2 wt%) no substantial differences in the hydration process were found. Replacement of cement with biochar resulted in the rise of the cement paste's yield stress, which is in line with observed workability tests for cement mortars. Higher replacement levels of cement with biochar significantly decreased workability of cement mortars. In the case of mechanical performance, biochar replacement with cement led to delays in the strength development of cement pastes and mortars. Mortar with 20 wt% of cement replacement with biochar showed 49% and 29% lower flexural and compressive strengths, respectively, compared to the control mortar. Due to the porous structure of biochar and extremely low density, cement mortars produced with biochar exhibited lower oven-dry density as well as substantially lower thermal conductivity. Replacement of 20 wt% of cement with biochar resulted in reduced thermal conductivity by 28% compared to the control sample. According to the durability assessments, replacing cement with biochar enhanced the freeze-thaw resistance of mortars by retaining the compressive strength loss and decreasing the surface cracks on the specimen. Moreover, improved acid resistance was found in specimens containing a high dosage of biochar. A series of thermal resistance tests showed that up to 300 °C, no substantial differences in the mechanical performance of mortars were found. However, beyond 300 °C, mortars with biochar experienced higher compressive strength losses, which can be attributed to the decomposition of biochar in the mortar and the porous matrix of the composite. In addition, biochar mixture had negative or close to zero heat of combustion. From the measured values of heat of combustion and results of cone calorimetry, it may be predicted that this material would be classified in A2 reaction to fire class. Finally, it was found that the presence of biochar in the mortar will not contribute to flame propagation.

Funding

This research was funded in part by the National Science Centre, Poland within Project No. 2020/39/D/ST8/00975 (SONATA-16).

CRediT authorship contribution statement

Pawel Sikora: Conceptualization, Methodology, Investigation, Validation, Visualization. Formal analysis, Data curation, Writing – original draft, Writing – review & editing, Project administration, Funding acquisition, Supervision, **Paweł Woliński:** Conceptualization, Methodology, Investigation, Resources, Formal analysis, Data curation, Visualization, Writing – review & editing, Visualization. **Mehdi Chougan:** Methodology, Investigation, Formal analysis, Data curation, Writing – original draft, Writing – review & editing. **Szymon Madraszewski:** Methodology, Investigation, Formal analysis, Data curation, Visualization, Writing – original draft, Writing – review & editing. **Wojciech Węgrzyński:** Methodology, Investigation, Formal analysis, Visualization, Writing – review & editing. **Bartłomiej K. Papis:** Investigation. **Karol Federowicz:** Investigation. **Seyed Hamidreza Ghaffar:** Investigation, Formal analysis, Writing – review & editing. **Dietmar Stephan:** Resources, Supervision, Writing – review & editing.

Declaration of Competing Interest

The authors declare that they have no known competing financial interests or personal relationships that could have appeared to influence the work reported in this paper.

Data Availability Statement

The data presented in this study are available on request from the corresponding author.

Acknowledgements

The authors would like to thank David Dahncke and Jessica Conrad from TU Berlin for conducting MIP and TGA studies, respectively. Moreover, authors thank Mateusz Techman and Daniel Sibera from the West Pomeranian University of Technology in Szczecin and Marta Sikora for support with rheological measurements, XRD analysis and data curation, respectively.

Appendix A. Supporting information

Supplementary data associated with this article can be found in the online version at doi:10.1016/j.indcrop.2022.115103.

References

Abd Elrahman, M., Chung, S.-Y., Sikora, P., Rucinska, T., Stephan, D., 2019. Influence of nanosilica on mechanical properties, sorptivity, and microstructure of lightweight concrete. Materials 12. https://doi.org/10.3390/ma12193078.

Ahmad, S., Khushnood, R.A., Jagdale, P., Tulliani, J.-M., Ferro, G.A., 2015. High performance self-consolidating cementitious composites by using micro carbonized bamboo particles. Mater. Design 76, 223–229. https://doi.org/10.1016/j.matdes.2015.03.048.

Akinyemi, B.A., Adesina, A., 2020. Recent advancements in the use of biochar for cementitious applications: a review. J. Build. Eng. 32, 101705 https://doi.org/10.1016/j.jobe.2020.101705.

Andrew, R.M., 2019. Global CO_2 emissions from cement production, 1928–2018. Earth Syst. Sci. Data 11, 1675–1710. https://doi.org/10.5194/essd-11-1675-2019.

Asadi, I., Shafigh, P., Abu Hassan, Z.F.B., Mahyuddin, N.B., 2018. Thermal conductivity of concrete – a review. J. Build. Eng. 20, 81–93. https://doi.org/10.1016/j.jobe.2018.07.002.

Asadi Zeidabadi, Z., Bakhtiari, S., Abbaslou, H., Ghanizadeh, A.R., 2018. Synthesis, characterization and evaluation of biochar from agricultural waste biomass for use in building materials. Constr. Build. Mater. 181, 301–308. https://doi.org/10.1016/j.conbuildmat.2018.05.271.

Babrauskas, V., 2017. Engineering variables to replace the concept of 'noncombustibility'. Fire Technol. 53, 353–373. https://doi.org/10.1007/s10694-016-0570-x.

Bashir, S., Zhu, J., Fu, Q., Hu, H., 2018. Comparing the adsorption mechanism of Cd by rice straw pristine and KOH-modified biochar. Environ. Sci. Pollut. Res. Int. 25, 11875–11883. https://doi.org/10.1007/s11356-018-1292-z.

Berra, M., Carassiti, F., Mangialardi, T., Paolini, A.E., Sebastiani, M., 2012. Effects of nanosilica addition on workability and compressive strength of Portland cement pastes. Constr. Build. Mater. 35, 666–675. https://doi.org/10.1016/j.conbuildmat.2012.04.132.

Bridgwater, A.V., 2012. Review of fast pyrolysis of biomass and product upgrading. Biomass Bioenergy 38, 68–94. https://doi.org/10.1016/j.biombioe.2011.01.048.

Cao, X., Huang, Y., Tang, C., Wang, J., Jonson, D., Fang, Y., 2020. Preliminary study on the electrocatalytic performance of an iron biochar catalyst prepared from iron-enriched plants. J. Environ. Sci. 88, 81–89. https://doi.org/10.1016/j.jes.2019.08.004.

Choi, W.C., Yun, H.D., Lee, J.Y., 2012. Mechanical properties of mortar containing biochar from pyrolysis. J. Korea Inst. Struct. Maint. Insp. 16, 67–74. https://doi.org/10.11112/jksmi.2012.16.3.067.

Chougan, M., Marotta, E., Lamastra, F.R., Vivio, F., Montesperelli, G., Ianniruberto, U., Bianco, A., 2019. A systematic study on EN-998-2 premixed mortars modified with graphene-based materials. Constr. Build. Mater. 227, 116701 https://doi.org/10.1016/j.conbuildmat.2019.116701.

Cleary, T., Quintiere, J., 1991. A framework for utilizing fire property tests. Fire Saf. Sci. 3, 647–656. https://doi.org/10.3801/IAFSS.FSS.3-647.

Clifton-brown, J.C., Stampfl, P.F., Jones, M.B., 2004. Miscanthus biomass production for energy in Europe and its potential contribution to decreasing fossil fuel carbon emissions. Glob. Change Biol. 10, 509–518. https://doi.org/10.1111/j.1529-8817.2003.00749.x.

Cuthbertson, D., Berardi, U., Briens, C., Berruti, F., 2019. Biochar from residual biomass as a concrete filler for improved thermal and acoustic properties. Biomass Bioenergy 120, 77–83. https://doi.org/10.1016/j.biombioe.2018.11.007.

Danish, A., Ali Mosaberpanah, M., Usama Salim, M., Ahmad, N., Ahmad, F., Ahmad, A., 2021. Reusing biochar as a filler or cement replacement material in cementitious composites: a review. Constr. Build. Mater. 300, 124295 https://doi.org/10.1016/j.conbuildmat.2021.124295.

Dixit, A., Gupta, S., Pang, S.D., Kua, H.W., 2019. Waste valorisation using biochar for cement replacement and internal curing in ultra-high performance concrete. J. Clean. Prod. 238, 117876 https://doi.org/10.1016/j.jclepro.2019.117876.

Dixit, A., Verma, A., Pang, S.D., 2021. Dual waste utilization in ultra-high performance concrete using biochar and marine clay. Cement Concr. Compos. 120, 104049 https://doi.org/10.1016/j.cemconcomp.2021.104049.

Gaunt, J.L., Lehmann, J., 2008. Energy balance and emissions associated with biochar sequestration and pyrolysis bioenergy production. Environ. Sci. Technol. 42, 4152–4158. https://doi.org/10.1021/es071361i.

Gupta, S., Kua, H.W., 2018. Effect of water entrainment by pre-soaked biochar particles on strength and permeability of cement mortar. Constr. Build. Mater. 159, 107–125. https://doi.org/10.1016/j.conbuildmat.2017.10.095.

Gupta, S., Kua, H.W., 2019. Carbonaceous micro-filler for cement: effect of particle size and dosage of biochar on fresh and hardened properties of cement mortar. Sci. Total Environ. 662, 952–962. https://doi.org/10.1016/j.scitotenv.2019.01.269.

Gupta, S., Kua, H.W., Tan Cynthia, S.Y., 2017. Use of biochar-coated polypropylene fibers for carbon sequestration and physical improvement of mortar. Cement Concr. Compos. 83, 171–187. https://doi.org/10.1016/j.cemconcomp.2017.07.012.

Gupta, S., Kua, H.W., Koh, H.J., 2018. Application of biochar from food and wood waste as green admixture for cement mortar. Sci. Total Environ. 619–620, 419–435. https://doi.org/10.1016/j.scitotenv.2017.11.044.

Haist, M., Link, J., Nicia, D., Leinitz, S., Baumert, C., Bronk, T., von, Cotardo, D., Eslami Pirharati, M., Fataei, S., Garrecht, H., Gehlen, C., Hauschildt, I., Ivanova, I., Jesinghausen, S., Klein, C., Krauss, H.-W., Lohaus, L., Lowke, D., Mazanec, O., Pawelczyk, S., Pott, U., Radebe, N.W., Riedmiller, J.J., Schmid, H.-J., Schmidt, W., Secrieru, E., Stephan, D., Thiedeitz, M., Wilhelm, M., Mechtcherine, V., 2020. Interlaboratory study on rheological properties of cement pastes and reference substances: comparability of measurements performed with different rheometers and measurement geometries. Mater. Struct. 53. https://doi.org/10.1617/s11527-020-01477-w.

Igalavithana, A.D., Mandal, S., Niazi, N.K., Vithanage, M., Parikh, S.J., Mukome, F.N.D., Rizwan, M., Oleszczuk, P., Al-Wabel, M., Bolan, N., Tsang, D.C.W., Kim, K.-H., Ok, Y. S., 2017. Advances and future directions of biochar characterization methods and applications. Crit. Rev. Environ. Sci. Technol. 47, 2275–2330. https://doi.org/10.1080/10643389.2017.1421844.

Kamm, J., 2004. A new class of plants for a biofuel feedstock energy crop. ABAB 113, 55–70. https://doi.org/10.1385/ABAB:113:1-3:055.

Kriker, A., Bali, A., Debicki, G., Bouziane, M., Chabannet, M., 2008. Durability of date palm fibres and their use as reinforcement in hot dry climates. Cement Concrete Compos. 30, 639–648. https://doi.org/10.1016/j.cemconcomp.2007.11.006.

L. Petersen, L., Lohaus, L., 2006. Entwicklung eines Prüfstandes für Parameterstudien zur Säurewiderstand von Hochleistungsbetonen. 16. Internationale Baustofftagung ibausil, Bauhaus-Universität Weimar, Tagungsbericht Band, 2.

Lehmann, J., Gaunt, J., Rondon, M., 2006. Bio-char Sequestration in terrestrial ecosystems – a review. Mitig. Adapt. Strat. Glob. Change 11, 403–427. https://doi.org/10.1007/s11027-005-9006-5.

Liu, R., Xiao, H., Guan, S., Zhang, J., Yao, D., 2020. Technology and method for applying biochar in building materials to evidently improve the carbon capture ability. J. Clean. Prod. 273, 123154 https://doi.org/10.1016/j.jclepro.2020.123154.

Lu, L., 2002. Char structural ordering during pyrolysis and combustion and its influence on char reactivity. Fuel 81, 1215–1225. https://doi.org/10.1016/S0016-2361(02)00035-2.

Maharaj, R., Grierson, L.H., Maharaj, C., Ramjattan-Harry, V., 2015. Rheological study of cement modified with a lignin based admixture. West Indian J. Eng. 68–73.

Mansuri, I., Farzana, R., Rajarao, R., Sahajwalla, V., 2018. Carbon dissolution using waste biomass—a sustainable approach for iron-carbon alloy production. Metals 8, 290. https://doi.org/10.3390/met8040290.

Mohan, D., Abhishek, K., Sarswat, A., Patel, M., Singh, P., Pittman, C.U., 2018. Biochar production and applications in soil fertility and carbon sequestration – a sustainable solution to crop-residue burning in India. RSC Adv. 8, 508–520. https://doi.org/10.1039/C7RA10353K.

Murugan, S., Gu, S., 2015. Research and development activities in pyrolysis – contributions from Indian scientific community – a review. Renew. Sustain. Energy Rev. 46, 282–295. https://doi.org/10.1016/j.rser.2015.02.050.

Ofori-Boadu, A.N., Kelley, R., Aryeetey, F., Fini, E., Akangah, P., 2017. The influence of swine-waste biochar on the early-age characteristics of cement paste. IJERA 07, 1–7. https://doi.org/10.9790/9622-0706010107.

Park, J.H., Kim, Y.U., Jeon, J., Yun, B.Y., Kang, Y., Kim, S., 2021. Analysis of biochar-mortar composite as a humidity control material to improve the building energy and hygrothermal performance. Sci. Total Environ. 775, 145552 https://doi.org/10.1016/j.scitotenv.2021.145552.

Praneeth, S., Saavedra, L., Zeng, M., Dubey, B.K., Sarmah, A.K., 2021. Biochar admixtured lightweight, porous and tougher cement mortars: mechanical, durability and micro computed tomography analysis. Sci. Total Environ. 750, 142327 https://doi.org/10.1016/j.scitotenv.2020.142327.

Qiu, Y., Liu, Z., Qian, L., Hao, J., 2017. Gaseous-phase flame retardant behavior of a multi-phosphaphenanthrene compound in a polycarbonate composite. RSC Adv. 7, 51290–51297. https://doi.org/10.1039/C7RA11069C.

Restuccia, L., Ferro, G.A., 2016. Promising low cost carbon-based materials to improve strength and toughness in cement composites. Constr. Build. Mater. 126, 1034–1043. https://doi.org/10.1016/j.conbuildmat.2016.09.101.

Restuccia, L., Ferro, G.A., Suarez-Riera, D., Sirico, A., Bernardi, P., Belletti, B., Malcevschi, A., 2020. Mechanical characterization of different biochar-based cement composites. Proc. Struct. Integrity 25, 226–233. https://doi.org/10.1016/j.prostr.2020.04.027.

Roberts, K.G., Gloy, B.A., Joseph, S., Scott, N.R., Lehmann, J., 2010. Life cycle assessment of biochar systems: estimating the energetic, economic, and climate change potential. Environ. Sci. Technol. 44, 827–833. https://doi.org/10.1021/es902266r.

Shafie, S., Salleh, M., Hang, L.L., Rahman, M., Ghani, W., 2012. Effect of pyrolysis temperature on the biochar nutrient and water retention capacity. J. Purity Util. React. Environ. 1 (6), 293–307.

Shen, Z., Tian, D., Zhang, X., Tang, L., Su, M., Zhang, L., Li, Z., Hu, S., Hou, D., 2018. Mechanisms of biochar assisted immobilization of Pb2+ by bioapatite in aqueous

solution. Chemosphere 190, 260–266. https://doi.org/10.1016/j.chemosphere.2017.09.140.
Sikora, P., Abd Elrahman, M., Stephan, D., 2018. The influence of nanomaterials on the thermal resistance of cement-based composites-a review. Nanomaterials 8. https://doi.org/10.3390/nano8070465.
Sirico, A., Bernardi, P., Belletti, B., Malcevschi, A., Dalcanale, E., Domenichelli, I., Fornoni, P., Moretti, E., 2020. Mechanical characterization of cement-based materials containing biochar from gasification. Constr. Build. Mater. 246, 118490 https://doi.org/10.1016/j.conbuildmat.2020.118490.
Song, W., Guo, M., 2012. Quality variations of poultry litter biochar generated at different pyrolysis temperatures. J. Anal. Appl. Pyrol. 94, 138–145. https://doi.org/10.1016/j.jaap.2011.11.018.
Strzałkowski, J., Sikora, P., Chung, S.-Y., Abd Elrahman, M., 2021. Thermal performance of building envelopes with structural layers of the same density: lightweight aggregate concrete versus foamed concrete. Build. Environ. 196, 107799 https://doi.org/10.1016/j.buildenv.2021.107799.
Suarez-Riera, D., Restuccia, L., Ferro, G.A., 2020. The use of biochar to reduce the carbon footprint of cement-based materials. Proc. Struct. Integrity 26, 199–210. https://doi.org/10.1016/j.prostr.2020.06.023.
Tan, K., Qin, Y., Du, T., Li, L., Zhang, L., Wang, J., 2021a. Biochar from waste biomass as hygroscopic filler for pervious concrete to improve evaporative cooling performance. Constr. Build. Mater. 287, 123078 https://doi.org/10.1016/j.conbuildmat.2021.123078.
Tan, K.-H., Wang, T.-Y., Zhou, Z.-H., Qin, Y.-H., 2021b. Biochar as a partial cement replacement material for developing sustainable concrete: an overview. J. Mater. Civ. Eng. 33, 3121001 https://doi.org/10.1061/(ASCE)MT.1943-5533.0003987.
Tomczyk, A., Sokołowska, Z., Boguta, P., 2020. Biochar physicochemical properties: pyrolysis temperature and feedstock kind effects. Rev. Environ. Sci. Biotechnol. 19, 191–215. https://doi.org/10.1007/s11157-020-09523-3.
van der Lugt, P., van den Dobbelsteen, A.A.J.F., Janssen, J.J.A., 2006. An environmental, economic and practical assessment of bamboo as a building material for supporting structures. Constr. Build. Mater. 20, 648–656. https://doi.org/10.1016/j.conbuildmat.2005.02.023.
Volk, T.A., Verwijst, T., Tharakan, P.J., Abrahamson, L.P., White, E.H., 2004. Growing fuel: a sustainability assessment of willow biomass crops. Front. Ecol. Environ. 2, 411–418. https://doi.org/10.1890/1540-9295(2004)002[0411:GFASAO]2.0.CO;2.
Wang, L., Chen, L., Tsang, D.C.W., Guo, B., Yang, J., Shen, Z., Hou, D., Ok, Y.S., Poon, C. S., 2020. Biochar as green additives in cement-based composites with carbon dioxide curing. J. Clean. Prod. 258, 120678 https://doi.org/10.1016/j.jclepro.2020.120678.
Wang, Q., Cui, X., Wang, J., Li, S., Lv, C., Dong, Y., 2017. Effect of fly ash on rheological properties of graphene oxide cement paste. Constr. Build. Mater. 138, 35–44. https://doi.org/10.1016/j.conbuildmat.2017.01.126.
Wu, F., Yu, Q., Liu, C., 2021. Durability of thermal insulating bio-based lightweight concrete: understanding of heat treatment on bio-aggregates. Constr. Build. Mater. 269, 121800 https://doi.org/10.1016/j.conbuildmat.2020.121800.
Yang, F., Zhang, S., Sun, Y., Tsang, D.C.W., Cheng, K., Ok, Y.S., 2019. Assembling biochar with various layered double hydroxides for enhancement of phosphorus recovery. J. Hazard. Mater. 365, 665–673. https://doi.org/10.1016/j.jhazmat.2018.11.047.
Yang, X., Lin, R.-S., Han, Y., Wang, X.-Y., 2021. Behavior of biochar-modified cementitious composites exposed to high temperatures. Materials 14. https://doi.org/10.3390/ma14185414.